Analytical Methods

Accepted Manuscript

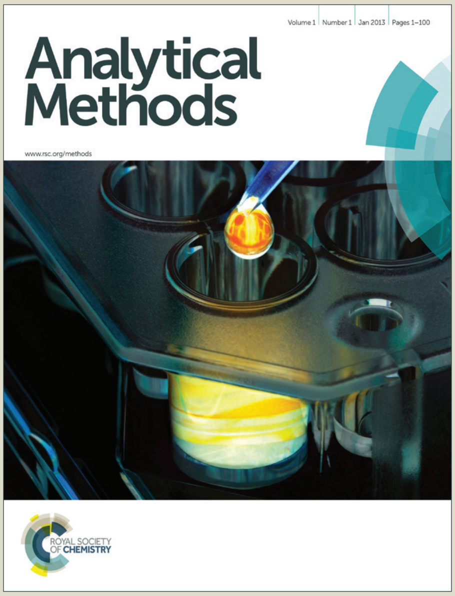

ROYAL SOCIETY OF CHEMISTRY

www.rsc.org/methods

Electrochemical Oxidation and determination of norepinephrine in the presence of acetaminophen using MnO_2 nano particles decorating reduced graphene oxide sheets

A.T. Ezhil Vilian, Shen-Ming Chen* Yu-Tsung Hung,

*Department of Chemical Engineering and Biotechnology, National Taipei University of Technology, No.1, Section 3, Chung-Hsiao East Road , Taipei 106, Taiwan (R.O.C).

*Corresponding author. Fax: +886 2270 25238; Tel: +886 2270 17147,
E-mail: smchen78@ms15.hinet.net

Abstract

In the present paper, a simple and rapid method for simultaneously measuring norepinephrine (NE) and acetaminophen (AC) that uses manganese dioxide particle decorated chemically reduced graphene oxide sheet nanocomposite electrodes is presented. The morphology and composition of the CRGO-MnO_2 nanocomposites are characterized by scanning electron microscopy (SEM), energy-dispersive X-ray spectroscopy (EDX), X-ray diffraction, Xray photoelectron spectroscopy (XPS) and Fourier transform infrared spectral techniques. The resultant CRGO-MnO_2 modified GCE electrode exhibited excellent electrocatalytic redox activities toward the NE. The experimental parameters for preparation of the CRGO-MnO_2 modified GCE also included variables related to simultaneous determination of NE and AC were optimized condition, at the same time, using square wave voltammetry (SWV). In particular, the peak potential separation between NE and AC at the CRGO-MnO_2 modified GCE electrode was as high as to 190 mV, much larger than that at the CRGO/GCE electrode. Using a square wave voltammetry, calibration curves for NE and AC were obtained over the range of 2×10^{-7} to 8×10^{-4} M and 4×10^{-6} to 8×10^{-3} with detection limits of 2.0×10^{-9} and 4.0×10^{-7} M, respectively. The proposed method was successfully applied to determine the NE and AC in samples with good results. In addition, the CRGO-MnO_2 modified GCE electrode has good reproducibility and high stability.

Keywords: Norepinephrine, Acetaminophen, MnO_2 Nanoparticles, Chemically reduced graphene oxide, Electrocatalysis.

1. Introduction

The adrenal medulla in the mammalian central nervous system secretes the important catecholamine, norepinephrine (NE). NE functions as a neurotransmitter, which is released as a metabotropic neurotransmitter from nerve endings in the sympathetic nervous system and some areas of the cerebral cortex.[1, 2] Norepinephrine plays an important role in health and disease.[3] In critical conditions, catecholamines can increase in association with stress, a fall in blood pressure or blood volume, thyroid hormone deficiency, congestive heart failure, or arrhythmias. Decreased amounts of catecholamines are seen in idiopathic postural hypotension.[4,5] Epinephrine, norepinephrine, and their metabolites are the primary indicators used for the diagnosis of catecholamine-secreting neurochromaffin tumors through laboratory measurements. In addition, NE accelerates HIV replication via the protein kinase because NE enhances adhesion of the human immunodeficiency virus-1 (HIV-1) infected leukocytes to cardiac micro vascular endothelial cells. [6] Thus, the quantitative determination of NE in biological fluids can provide important information about physiological functions and aid in the clinical diagnosis of some diseases. Various methods, including spectrophotometry, capillary electrophoresis, gas chromatography, and high-performance liquid chromatography (HPLC) have been employed for the determination of NE. However, NE is an electro active compound that can be oxidized electrochemically, so the development of electrochemical sensors for the determination of NE has been the focus of research over the past few decades. Electrochemical methods have several advantages over other methods such as being inexpensive and simpler procedures, high sensitivity, reproducibility and ease of miniaturization. [7]

Paracetamol (acetaminophen) is an antipyretic drug that is a safe and effective painkiller used for the widespread relief of moderate pain associated with backache, headache, arthritis and postoperative pain. [8, 9] However, overdoses of paracetamol can lead to liver and kidney damage and even death. It is also worth noting that some epidemiological studies suggest a possible association between the use of paracetamol during pregnancy and the increased appearance of asthma in children. [10] Furthermore, paracetamol might be reentering the food chain through contaminated feather meal, which can be used as an additive in animal feed. [11] Thus, it is imperative to develop a simple, fast and accurate quantification method for paracetamol, as it can directly impact clinical diagnosis, food safety and the quality of paracetamol-containing medicines. [12] Several different methods used for the determination of paracetamol have been reported in the literature, including liquid chromatography spectrophotometry, chemiluminescence, capillary electrophoresis, amperometric batch injection analysis, colorimetry, titrimetry, FTIR and Raman spectrometry and flow injection analysis (FIA). The electrochemical method, however, has attracted significant attention as an alternative method because of its inherent advantages of simplicity, high sensitivity and relatively low cost. [13, 14]

For the past few decades, graphene has been used as an advanced material in nanotechnology because of its unique electronic, optical and chemical properties and has attracted tremendous attention for many potential applications. [15] Importantly, large amounts of substances including a wide range of metals, nanoparticles, biomolecules, and drugs, can easily cause the immobilization of large amount of substances on graphene oxide (GO). This is one of the most important derivatives of graphene, with a two-dimensional plane and oxygen functional groups along the basal planes and edges, which provide it with a large specific surface area.[16] Recently, the two-dimensional (2D) structure of sp^2-bonded carbon materials has drawn considerable interest for its fascinating properties and wide applications and the fact that it has an ultra high surface area of up to 2630 m^2 g^{-1}, and excellent conductivity. [17]

In recent years, remarkable advances have been achieved in creating composites of graphene and manganese dioxide (MnO_2) with an improved capacitance. [18,19] MnO_2 which is an important metal oxide with distinctive properties has found wide applications in catalysis, molecular adsorption, biosensor, and energy storage. [20] MnO_2 has also enabled the employment of catalytic substance for a variety of electrochemical applications due to its low cost, high activity, and lack of toxicity. [21]

To the best of our knowledge, no study has reported on a simple and sensitive method for simultaneously measuring NE and AC. Thus, we develop an electrochemical sensor using a novel method with where manganese dioxide particles decorate reduced graphene oxide sheets are used to fabricate a modified glassy carbon electrode through a simple electrode positioning method. This work describes a simple, reliable, and an inexpensive electrochemical sensor for simultaneous determination of NE and AC using the square wave voltammetry (SWV) technique. The results indicate that the CRGO-MnO_2 modified electrode remarkably enhances the oxidation signal of NE and AC when SWV is adopted, and obviously lowers the oxidation potential of these compounds. Therefore, there is good separation of the oxidation peaks of NE and AC at the CRGO-MnO_2 modified electrode. The calibration curves for NE and AC were acquired in the range of 2×10^{-7}-8×10^{-4} and 4×10^{-6}-8×10^{-3} M with detection limits (S/N = 3) of 2.0×10^{-9} M and 4.0×10^{-7} M, respectively. A sensitive and rapid electrochemical method for simultaneous determination of NE and AC was set up for routine analysis.

2. Experimental Procedure

2.1. Reagents

Norepinephrine, acetaminophen, H_2SO_4, Na_2HPO_4 and NaH_2PO_4, *N*,*N*-dimethylformamide (DMF) were purchased from Sigma-Aldrich. Shimakyu, Osaka, Japan, kindly supplied the $KMnO_4$ reagent. All reagents used in this study were of analytical grade and used as purchases. The aqueous electrolyte solutions were prepared in a 0.05 M phosphate buffer solution (PBS) which was made from Na_2HPO_4. NaH_2PO_4 was used as the supporting electrolyte and the pH values were adjusted with the addition of 0.1 M HCl or NaOH solutions. Stock solutions of norepinephrine and acetaminophen were freshly prepared daily by dissolving suitable amounts of water. Working solutions containing the chemical substances were prepared daily by appropriate dilution of the stock solutions with water. All measurements were carried out at room temperature. All aqueous solutions were freshly prepared with double distilled and sterilized water.

2.2. Apparatus

Cyclic voltammetry, square wave voltammetry and All electrochemical measurements were performed on a CH Instrument 405Aelectrochemical analyzer (Shanghai Chenhua Co., China) using a three electrode arrangement, equipped with a platinum wire counter electrode, a saturated Ag/AgCl/KCls electrode as the reference electrode and the CRGO-MnO_2 modified GCE electrode as the working electrode. The prepared electrodes with the MnO_2, CRGO and CRGO-MnO_2 modified films were characterized by scanning electron microscopy (SEM), which was performed with a Hitachi S-3000 H and energy-dispersive X-ray spectroscopy (EDX) recorded using a HORIBA EMAX X-ACT Model 51-ADD0009. Electrochemical impedance spectroscopy (EIS) was carried out at a frequency range of 100 kHz to 1.0 Hz with a ZAHNER instrument (Kroanch, Germany). X-ray diffraction (XRD) analysis was taken by an XPERT-PRO diffractometer (PANalytical B.V., the Netherlands) using Cu Kα radiation (k =1. 54 A◦). X-Ray photoelectron spectroscopy (XPS) was carried out with a PHI 5000 Versa Probe equipped with an Al Kalpha X-ray source (1486.6 eV). The Fourier transform infrared (FTIR) spectra were determined using a Perkin Elmer RXI spectrometer.

2.3. Procedures

2.3.1. Preparation of the CRGO

The preparation procedure (the modified Hummer's method) for graphene oxide has been described in a previous study. [22, 23] Briefly, 46 ml of H_2SO_4 were added to a mixture of 1 g of graphite (graphite powder, <20 µm, Aldrich) then stirred in a round bottom flask at 0 °C for 15 min. Next, a 6 g portion of $KMnO_4$ and 1 g of $NaNO_3$ in 31.2 ml of water were added gradually while stirring. The temperature of the mixture was maintained below 20 °C. Next, the sample was stirred at 35 °C for 2 h, after which 500 ml of distilled water was added slowly to keep the temperature below 50°C. After that, further reaction, 250 ml of water and 6 ml of H_2O_2 (30 weight %) were added. The color of the mixture changed to brilliant yellow. Finally, the solid suspension was washed using 2 M of HCl solution and then washed 3-4 times with ethanol and dried in a vacuum at 60 °C overnight. The graphite oxide slurry was then dried in a vacuum oven at 60 °C for 48 h before use. Afterwards, a 0.5g mg mL^{-1} graphene oxide sample was prepared by dispersing it in DMF with the aid of ultrasonication for 30 minutes. The CRGO sample was prepared by mixing 20 mg of graphite oxide with 40 ml of 50mM aq. $NaBH_4$ for 1 h. Thereafter, the mixture was ultrasonicated for 1 h. The CRGO dispersion was then washed with water and dried at 60 °C for 48 h in a vacuum oven. Afterwards, a sample of CRGO (0.5g mg mL^{-1}) was prepared by dispersing in DMF with the aid of ultrasonication for 30 minutes.

2.3.2. Preparation of the CRGO-MnO_2 modified GCE electrodes

The glassy carbon (GCE) electrode was first polished with an alumina (particle size of about 0.05 mm)/water slurry using a Buehler polishing kit. Then the GCE electrode (3mm in diameter) was thoroughly washed with water and cleaned in an ultrasonic bath for about 5min with pure water. A volume of 5µL of the CRGO suspended in liquid was coated on the cleaned GCE electrode and dried in air for about 2 h. Under the optimum conditions, 1 mg/ml of CRGO would be used. Higher amounts of CRGO could agglomerate on the electrode surface which would affect the catalytic activity and stability. Hence, 1 mg/ml of CRGO was used to improve the electrochemical catalysis. Subsequently, cyclic voltammetry (CV) was used to examine the MnO_2 electrochemically deposited on the CRGO modified electrode surface following a previously reported procedure. [24] The CV of the MnO_2 electrode position was performed consecutively for 2 cycles over an optimized potential range of 0.5 V and -0.3 V at a scan rate of 2 mV s^{-1} in a 10 mm $KMnO_4$ + 0.04 M H_2SO_4 aqueous solutions. Finally, the CRGO-MnO_2 modified GCE electrodes were rinsed with water and used for electrochemical catalysis studies.

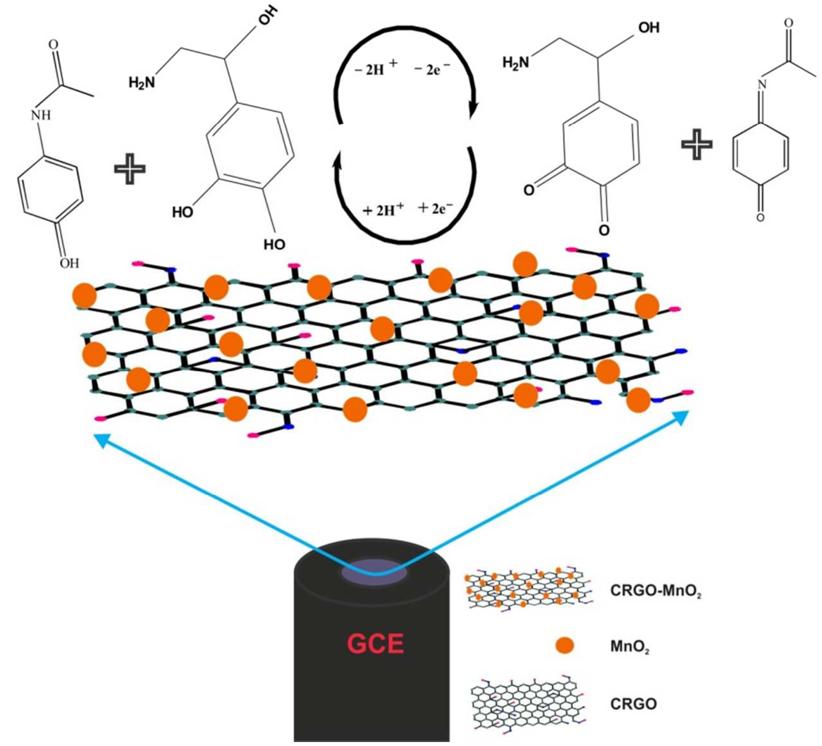

Schematic representation of Electrochemical Oxidation and Determination of norepinephrine and acetaminophen based on the CRGO-MnO_2 film modified electrode.

3. Results and discussion

3.1 XPS analysis

The chemical composition of the CRGO-MnO_2 sheets can be further determined by XPS measurements, as shown in Fig. 1A. The wide scan XPS spectra of the CRGO-MnO_2 composites (Fig. 1A) clearly indicate that the sample was composed of C, Mn, and O, with no peaks for other elements observed. Fig. 1A shows the combined CRGO-MnO_2 XPS spectrum for the elements present in the prepared sample. The high-resolution spectra of the C1s can be fitted to three peaks indicated binding energies of 284.80, 286.32 and 288.38 eV respectively, implying the existence of three different chemical environments of carbon in the sample. The peak at 284.80 eV can be assigned to the contributions of the C-C (sp^2) bonds, while the peak at

286.32 eV is due to the existence of C-OH bonds and the peak at 288.38 eV comes from the existence of C-OOH bonds (See,Fig.1B). Moreover, the measured peaks at 642.2 eV and 653.8 eV can be assigned to the Mn 2p. Fig.1C shows the XPS spectra for the Mn 2p decorating the CRGO surface. The Mn 2p spectra contain two peaks, namely Mn $2p^{3/2}$ and Mn $2p^{1/2}$. For Mn 2p, the measured peak at 642.2 eV corresponds to the binding energy of Mn 2p $^{3/2}$ and the peak at 653.8 eV corresponds to Mn 2p $^{1/2}$, with a spin-energy separation of 11.6 eV, which matches the value reported in past work. [25, 26] In addition to this, there are two shakes up peaks demonstrating the formation of Mn nanoparticles on the surface of the CRGO by a simple electrochemical method, as shown in Fig.1C. All the observations confirm the successful preparation of CRGO-MnO_2 composites.

Fig. 1

3.2 FTIR spectroscopy and SEM and EDX analysis

Fig.1D shows the FTIR spectroscopic analysis of (a) GO and (b) CRGO-MnO_2 nanoparticle composite powders. The GO spectrum is in good agreement with that reported in the literature. [27] The peaks at 3500 and 1250 cm^{-1} are attributed to the stretching of the O-H bonds. The peaks at 1730 and 1620 cm^{-1} are associated with the stretching of the C=O and C=C bonds. The peaks at 1220 and 1100 cm^{-1} are associated with the C-O bonds of the carboxyl groups. The FTIR spectrum of CRGO-MnO_2 shows evidence of the dramatic weakening of the peak at 3500 cm^{-1}. It can be observed from Fig.1D (curve a) that the GO exhibits several characteristic absorption bands of oxygen-containing groups. A vibrational band at around 1497 cm^{-1} can be assigned to the complex formations between the carboxyl group and Mn on the surface of the magnetic particles, indicating that the MnO_2 nanoparticles are bound to the CRGO surface (curve b). [25]

Fig. 2

Fig. 2 shows the morphology of the samples based on SEM and EDX images of CRGO (A&D), MnO_2 (B&E), and CRGO-MnO_2 (C&F). Fig.2A and D clearly show the typical wrinkled structure of the chemically reduced graphene oxide caused by sheet folding. The results of EDX analysis corresponding to the elements of C (80%) and O (20 %), respectively, are shown. The morphology of the MnO_2 nanoparticles can also be seen in the Fig.2B. MnO_2 shows the nanoparticle morphology. The EDX spectrum shows peaks corresponding to the elements, Mn (55%) and O (45%), confirming the deposition of Mn nanoparticles on the ITO surface (See Fig.2E). On the other hand, the CRGO sheets are still wrapped around the MnO_2 nanoparticles. Since CRGO contains a wide range of oxygen functional groups, it is expected to lead to direct interaction, such as hydrogen bonding or a dehydration reaction between the surface oxygen of the MnO_2 nanoparticles and the CRGO (See Fig.2C). The corresponding EDX spectra for CRGO-MnO_2 appearing in Fig. 2F show peaks corresponding to the elements of C (10%), O (65), and Mn (25%), confirming the existence of metallic Mn nanoparticles on the surface of the CRGO nanosheets. Furthermore, due to the large crumpled surface area of the CRGO nanosheets, Mn nanoparticles can be deposited on both sides. This high deposition rate of MnO_2 nanoparticles onto the surface of the CRGO due to the large surface area will be beneficial to improving the catalytic activity and sensor sensitivity.

3.3 CV and EIS characterization of the modified electrode interface

The performance of the bare GCE, MnO_2, CRGO and the CRGO-MnO_2 modified GCE was evaluated by cyclic voltammetry in 0.05 M phosphate buffer solutions (pH 7.0) containing 5mM $Fe(CN)_6^{3-/4-}$as probes. As seen in Fig. 3A, there is a pair of redox wave at the CRGO/GCE interface with a peak-to-peak separation (ΔE) of 72 mV (curve d), suggesting the fast electron transfer kinetics of the Fe (CN) $_6^{4-/3-}$ redox probe. This value was smaller than the value of 94 mV obtained for the bare GC electrode under the same experimental conditions. There was a remarkable increase in the ΔE value when the value of 140 mV for MnO_2 was modified on the CRGO/GCE surface. Compared with the MnO_2 (curve a), the MnO_2/CRGO/GCE (curve b) films presented an increased current because the MnO_2 possess excellent conductivity properties and effectively promote electron transfer between the electrolyte and the electrode surface. On the other hands, Fig. 3A shows that MnO_2 (curve a) block the redox process of the redox probe in the solution.These results indicate that the CRGO-MnO_2 modified GCE can improve the redox of the probe, which is attributed to be quasi-reversible (peak-to-peak separation larger than 100 mV) with the best diffusion-controlled behavior of MnO_2/CRGO/GCE electrode.

Fig. 3

On the other hand, as can be seen in Fig. 3B, EIS is an effective method for probing the features of surface-modified electrodes. In EIS, the diameter of the semicircle in the impedance spectrum is equal to the electron-transfer resistance, R_{et}. This resistance controls the electron transfer kinetics of the redox probe ([Fe (CN) $_6]^{4-/3-}$) at the electrode interface. At the bare GC electrode, the redox process of the probe showed a R_{et} of about R_{et} (360 Ω). When MnO_2 modified the GCE, there was a decrease in the interfacial $R_{\mathbf{et}}$ (180 Ω) compared to that of the bare GCE. After the MnO_2 modification of the GCE, it became almost a straight line, which is a characteristic of diffusion limited electrochemical processes.Furthermore, The CRGO modified

GCE electrode exhibited a smaller R_{et} (578 Ω) for the redox probe, because of the electrostatic repulsion between the negatively charged surface of the CRGO and the probe molecules. Furthermore, the EIS exhibits a very High interfacial R_{et}, indicating that the resulting CRGO greatly enhanced electron transfer at the redox probe. With further electro deposition of MnO_2 nanoparticles onto the CRGO modified GCE electrode, the R_{et} (120 Ω) decreased, which indicates the good conductivity of the MnO_2 particles that could make electron transfers easier. This indicates that the modified $MnO_{2/}$CRGO modified GCE displayed much less interfacial transfer resistance than the bare GCE. However, subsequent attachment of MnO_2 onto the CRGO modified GCE lead to a great decrease of R_{et}. This may have been because of the acceleration of electron transfer of MnO_2 between contacts, through the CRGO modified GCE, which thus provides high electron transfer ability.

3.4 Cyclic voltammetric behavior of NE and AC at the CRGO-MnO_2 modified GCE

The electrochemical behavior of the bare GCE, $MnO_{2,}$ CRGO and the CRGO-MnO_2 modified GCE was investigated via cyclic voltammetry. Fig.4A shows the cyclic voltammograms in a co-existence system of NE and AC for the bare GCE, $MnO_{2,}$ CRGO and CRGO-MnO_2 modified GCE 0.05M PBS (pH 7.0). For the bare GCE and $MnO_{2,}$ the oxidation peaks of NE and AC completely overlap, and the peak potentials for NE and AC are indistinguishable, which reveal that it is impossible to simultaneously determine these compounds with bare GCE and $MnO_{2,}$ and modified GCE electrodes. Furthermore, the CRGO modified GCE also leads to an enhancement in the current response. However, the NE and AC compounds cannot be effectively separated based on the small oxidation peak potential differences and poor current responses with the CRGO modified GCE. However, the presence of

MnO_2 nanoparticles on the CRGO modified GCE surface may improve the catalytic activity for the oxidation of NE and AC. The enhanced current response and the lowered over potential clearly indicate that the rate of electron transfer can be accelerated by the addition of the CRGO-MnO_2 modified GCE film, leading to excellent electrocatalytic activity favoring the oxidation of NE and AC. In contrast to the CRGO-MnO_2 modified GCE, this can be attributed to the high surface area, excellent catalytic activity and good conductivity of graphene. This method can offer special approaches to the simultaneous electrochemical determination of oxidized NE and AC at 0.23 and 0.42 V, respectively. Obviously, this separation was good enough to achieve the simultaneous determination of NE and AC in a mixture solution.

Fig. 4

3.5 Effect of scan rate

The influence of the scan rate of the electrocatalytic activity of the CRGO-MnO_2 modified GCE electrodes in pH 7.0 PBS containing 1×10^{-4} M NE and 1×10^{-4} M AC was investigated using CV (Fig.S1). It can be seen that the anodic peak current increases with the increase of the scan rate and there is a good linear relationship between the anodic current and scan rate in the range from 10 to 100 mV/s^{-1}. Both the cathodic peak current (I_{pc}) and anodic peak current (I_{pa}) of AC and NE increased linearly with the scan rate. The linear dependence of I_{pc} and I_{pa} on the scan rate is shown in the inset in Fig. S1. This demonstrates that an adsorption-controlled process with two-electrons and two protons controlled the redox process for NE and AC at the CRGO-MnO2 modified GCE electrode.

3.6 Effect of solution pH

The influences of the buffer pH on the current responses of the 1×10^{-4} M NE and 1×10^{-4} M AC at the CRGO-MnO_2 modified GCE surface were investigated CV for a pH ranging from 3.0 to 9.0. As can be seen in Fig. S2, the anodic peak currents of NE and AC increased slowly as the pH rose from 3.0 to 9.0 but when the pH exceeded 7.0, the anodic peak current decreased rapidly. The influence of the pH on the anodic peak potential (E_{pa}) for the CRGO-MnO_2 was also investigated and the results are shown in Fig. S2. One can see a negative shift in all the anodic peak potentials with an increase in the pH from 3.0 to 9.0. for both NE and AC. The equations for determining the peak potential with the pH are E_{pa} = -0.0584+0.6999 pH ($R^2 = 0.9932$) and E_{pa} = -0.055+0.8965 pH ($R^2 = 0.9971$) for NE and AC, respectively. The slopes of the two regression equations are very close to the theoretical value of 59 mV/pH, suggesting that the number of electrons and protons taking part in the electrode reaction are equal. [28] Thus, the electrochemical oxidation of NE and AC at the CRGO-MnO_2/GCE is likely to be a two-electron and two-proton process. Consequently, the determination sensitivity and the electrochemical responses of NE and AC are best peak separated (190 mV). Therefore, it can be seen that pH 7.0 PBS should be selected as the supporting electrolyte for optimal experimental conditions. The probable electrode reaction is shown in Scheme 1.

3.7 Simultaneous determination of NE and AC

Fig. 4B shows the SWV used for differentiation in the oxidation peak potentials for NE and AC which is large enough for the separation and simultaneous determination of NE and AC with the CRGO-MnO_2 modified GCE electrodes, because of the high current sensitivity and very low detection limit. As shown in Fig.4B, The SWV results indicate the simultaneous determination of NE and AC with two well distinguished anodic peaks with potentials of 230mV and 420 mV, corresponding to the oxidation NE and AC, respectively. The separation between the NE and AC oxidation peaks was about 190 mV. The results show that the peak separation was sufficient with the CRGO-MnO_2 modified GCE electrode. The peak currents increased linearly with increasing NE and AC concentrations ranging from 2×10^{-7}-8×10^{-4} and 4×10^{-6}-8×10^{-3} M with a lower detection limit of 2.0×10^{-9} and 4.0×10^{-7} M, at a signal-to-noise ratio of (S/N=3) (Fig. 4B). The sensitivity to NE and AC of the CRGO-MnO_2 modified GCE electrode was calculated to be 60.2 mA mM^{-1} cm^{-2}, which is much higher than that of the NE sensor based on carbon based electrodes. A comparison of the proposed method to the reported ones, presented in Table 1, indicates that the proposed method is superior to the previous ones with regard to detection limit and linear concentration range. The SWV results show higher sensitivity and better resolution than for cyclic voltammetry.

Fig. 5

Fig. 5A, the SWV obtained for increasing various concentrations of AC in the presence of 200 μM NE show that the oxidation peak current increases linearly with increasing concentrations of AC in the range of 6.0×10^{-6} to 7.0×10^{-4} M. No obvious change in the NE peak currents was observed when the concentration of AC was varied. The following linear equation: Ipc (μA) = 1.520×10^{-7} + 0.02483C (AC) with a linear relative coefficient of R^2 = 0.9982,was obtained. The detection limit for AC was 1.0×10^{-6} M (S/N = 3).Similarly, in Fig. 5B shows the results of SWV experiments carried out either by varying the oxidation processes of NE concentration in the presence of 200 μM AC or by varying the AC concentration in the presence of 200 μM NE in the pH 7 PBS. The results show that i_{pa} was proportional to the concentration of NE in the linear range of 2×10^{-7}-8×10^{-4} M. The regression equation is Ipa (μA) = 5.689×10^{-8} + 0.01822 C with a linear relative coefficient of R^2 = 0.9923, and the detection limit is 1.0×10^{-6}

mol L^{-1} (S/N = 3). It can be seen that there was an excellent SWV response, with the signal height of the other AC remaining unchanged. Thus, the selective and sensitive determination of NE and AC was achieved simultaneously at this CRGO-MnO_2 modified GCE electrode.

3.8. Effect of the accumulation potential and the accumulation time

The effect of the accumulation potential (E_{acc}) on the SWV anodic peak currents of NE and AC in a mixed solution of 0.05 M pH 7.0 PBS was investigated over the range of 0 to 0.6 V, as shown in Fig. S3. The increase in anodic peak current with increasing accumulation potential might be due to the electrostatic interaction between the NE and AC with the electron rich electrode that occurs at this potential. However, at higher accumulation potentials than 0.3 V there was a gradual decrease in the peak current, although this was not statistically significant. Accordingly, 0.3 V was selected as the optimum accumulation potential.

The accumulation time was considered in relation to the square wave voltammetric peak currents for mixed solutions of 1×10^{-4} M NE and 1×10^{-4} M AC in 0.05 M pH 7.0 PBS. The range examined was 0-240 s. The results are presented in Fig. S4. As the accumulation time was increased the peak current also increased until reaching a maximum value at 120 s for both NE and AC and then decreasing as the accumulation time increased further (See Fig. S4), indicating saturation of the electrode surface. Therefore, an accumulation time of 120 s was selected. SWV was used for the determination of NE and AC at the CRGO-MnO_2 modified electrode because of its higher current sensitivity and better resolution than CV.

3.9 Stability and reproducibility

The reproducibility and stability of the CRGO-MnO_2 modified electrode were investigated through SWV measurements (0.05 mM NE and AC). Using four different electrodes, the relative standard deviation (R.S.D.) was about 3.4%. The stability was also measured after storing the CRGO-MnO_2 modified electrode in 0.05 M PBS (pH 7.0) at 4 °C. There was no apparent decrease in the current response for NE, while for AC, 91% of its initial value after 30 days and about 78% after 50 days.These results demonstrate that the CRGO-MnO_2 modified electrode has good reproducibility and stability and provides a very stable environment for the detection of NE and AC.

The CRGO-MnO_2 modified electrode was then utilized for SWV determination of the concentration of NE in injection samples and paracetamol tablets. A real sample was purchased from a near by pharmacy/hospital and utilized for the sample analysis. The adrenaline injection and paracetamol tablets were dissolved in pH 7 PBS solutions before measurements were taken. The SWV responses for the NE and AC recorded at the CRGO-MnO_2 modified electrode are displayed in Table S1. The NE and AC content was estimated using the standard addition method. The recovery ratio indicates that the present method is reliable and suitable for the determination of NE and AC in spiked samples. The results for the determinations of NE and AC in urine samples are listed in Table S2. The obtained urine sample was diluted 10 times with a phosphate buffer solution of pH 7 and the samples were spiked with specified concentrations of NE and AC. Measurements were made for determination of the NE and AC concentrations in the urine samples. The results presented in Table 2 indicate that the modified electrode retained its efficiency for the determination of NE and AC in real samples with satisfactory results. The results show that CRGO-MnO_2 can be successfully employed for the determination of NE and AC in real samples.

4. Conclusion

In this work, we report on the fabrication of a CRGO-MnO_2 composite which was applied to construct a modified electrode. Anchored MnO_2 nanoparticle were uniformly deposited on the surface of the CRGO. We have shown that the CRGO-MnO_2 film modified glassy carbon electrode exhibits highly electrocatalytic activity in regards to the oxidation of NE and AC with a low detection limit and good linear range. The results demonstrate that the oxidation of NE and AC at the surface of CRGO-MnO_2 occurs at potentials of about 230 and 420 mV, which is more negative than for the bare GCE. It was an adsorption-controlled process with two electrons and two protons. The modified electrode not only improved the electrochemical catalytic oxidation of NE and AC, but also resolved the overlapping anodic peaks. Furthermore, the proposed sensor demonstrated selectivity, sensitivity, excellent stability and reproducibility towards the detection of NE and AC. Our proposed method is confirmed to have good accuracy for detection in urine and pharmaceutical samples and should be suitable for practical applications.

Acknowledgements

The National Science Council and the Ministry of Education of Taiwan (Republic of China) supported this work

References

1. M. Mohseni, M. Alibeik, A. Benvidi, *Sens. Actuators, B*, 2012, **171,**380-386.

2. S. Huang, H. Liao, D. Chen, *Biosens. Bioelectron*., 2010, **25,** 2351-2355.

3. D. Voet, J.G. Voet, Biochemistry (2nd ed.) Wiley, New York (1995).

4. M. Ardakani, M. Mohseni, M. Alibeik, *J. Mol. Liq.,* 2013, **178,**63-69.

5. M. Ardakani, H. Beitollahi, M. Mohseni, H. Naeimi, N. Taghavinia, *Appl. Catal. A: Gen.,* 2010, **378,** 195-201.

6. S. W. Cole, Y.D. Korin, J.L. Fahey, J.A. Zack, *J. Immunol.,* 1998, **161,** 610-616.

7. S. Salmanpoura, T.Tavanab, A. Pahlavanc, M. Khalilzadehd, A. Ensafie, H. Malehd, H. Beitollahif, E. Kowsarig, D. Zareyeeb, *Mater. Sci. Eng. C.*, 2012, **32,**1912-1918.

8. W.Y. Su, S.H. Cheng, *Electroanalysis*, 2010, **22,** 707-714.

9. A. Khaskheli, J. Fischer, J. Barek, V. Vyskočil, Sirajuddin, M. Iqbal Bhanger, *Electrochim. Acta*., 2013,**101**, 238-242.

10. T. Canevari, P. Pereira, R. Landers, E. Benvenutti, S. Machado, *Talanta*, 2013,**116,**726-735.

11 H. Ghadimi, R. Tehrani, A. Ali, N. Mohamed, S. Ghani, *Anal. Chim. Acta*, 2013,**765,** 70-76.

12. Y. Li, S. Feng, S. Li, Y. Zhanga, Y. Zhonga, *Sens. Actuators, B*, 2014, **190,** 999-1005.

13. L. Svorc, J. Sochra, P. Tomcík, M. Rievaja, D. Bustina, *Electrochim. Acta*., 2012, **68,**227-234.

14. B. LourenCoa, R. Medeiros, R. Filhob, L. Mazoa, O. Filho,*Talanta,* 2009,**78,**748-752.

15. S. Palanisamy, S. Chen, R. Sarawathi, *Sens. Actuators, B*, 2012,**166,**372-377.

16. B. Unnikrishnan, S. Palanisamy, S. Chen, *Biosens. Bioelectron*., 2013, **39,** 70-75.

17. J. Liu, L. Cui, D. Losic, *Acta Biomaterialia*,2013, **9,** 9243-9257.

18. L. Zhang, S. Yuan, L. Yang, Z. Fang, G. Zhao, *Microchim. Acta*, 2013,**180,**627-633.

19. X. Wang, Y. Li, *J Am Chem Soc*., 2002, **124,**2880-2881.

20. Y. Luo,.*Mater Lett.,* 2007,**61,**1893-1895.

21. L. Li, Z. Du, S. Liu, Q. Hao, Y. Wang, Q. Li , T. Wang, *Talanta*, 2010, **82,**1637-1641.

22. D. Marcano, D. Kosynkin, J. Berlin, A. Sinitskii, Z. Sun, A. Slesarev, L. Alemany, W. Lu, J. Tou, *ACS Nano*, 2010, **4,** 4806-4814.

23. V. Mani, A. Periasamy, S. Chen, *Electrochem. Commun*., 2012,**17,** 75-78.

24. B. Unnikrishnan, P. Ru, S. Chen, *Sens. Actuators, B*, 2012, **169,** 235-242.

25. Z. Li, Y. Mi, X. Liu, S. Liu, S. Yang, J. Wang, *J. Mater. Chem*., 2011, **2,**14706-14711.

26. K. Ye, Z. Liu, C. Xu, N. Li, Y. Chen, Y. Su, *Inorg. Chem. Commun*., 2013,**30,**1-4.

27. C. Hou, H. Quan, Y. Duan, Q. Zhang, H. Wang, Y. Li, *Nanoscale*, 2013,**5,** 1227-1232.

28.C. Bian,Q.Zeng,H.Xiong,X.Zhang,S.Wang,*Bioelectrochemistry*, 2010, **79,** 1-5.

29. H. L. Zhang, Y. Liu, G.S. Lai, A.M. Yu, Y.M. Huang, C.M. Jin, *Analyst*, 2009, **134,** 2141-2146.

30. M. Reza Akhgar,H.Beitollahi,M. Salari, H. Karimi-Maleh, H. Zamani, *Anal. Methods*, 2012, **4,** 259.

31.Rosy, S.K. Yadav, B. Agrawal, M. Oyama, R.N. Goyal, *Electrochim. Acta*.,2014, **125,** 622-629.

32. M.Mazloum-Ardakani, A.Khoshroo, *J. Electroanal. Chem*., 2014, **718,**17-23.

33. N. Nasirizadeh, H.R. Zare,*Talanta*, 2009,80, 656-663.

34. A.R. Taheri, A. Mohadesi, D. Afzali, H. Karimi-Maleh, H. Mahmoudi Moghaddam, H. Zamani, Z. Rezayati zad, *Int. J. Electrochem. Sci*. 2011,**6,** 171-180.

35.X. Ma, M. Chen, X. Li, A. Purushothaman, F. Li, *Int. J. Electrochem. Sci*, 2012,**7,** 991-1000.

36.H. Yao, S. Li, Y. Tang, Y. Chen, Y. Chen, X. Lin, *Electrochim. Acta*, 2009, **54,** 4607-4612.

37. S. Salmanpour, T. Tavana, A. Pahlavan, Md. A. Khalilzadeh, A.A. Ensafi, H. Karimi-Maleh, H. Beitollahi, E. Kowsari, D. Zareyee, *Mater. Sci. Eng. C.*, 2012,**32**,1912-1918.

38. H.Beitollahi, S. Mohammadi, *Mater. Sci. Eng. C.*, 2013, **33,**3214-3219.

39. M. Amiri-Aref, J. B. Raoof, R. Ojani, *Sens. Actuators, B*, 2014,**192,**634-641.

Fig. captions

Fig 1. (A) XPS results for MnO_2 /CRGO; (B) Mn 2p core-level XPS spectra of MnO_2/CRGO.

(c) FT-IR spectra of the (a) GO and (b) MnO_2/CRGO.

Fig 2. SEM images of (A) CRGO, (B) MnO_2, (C) MnO_2/CRGO, and EDX spectra of (D) CRGO, (E) MnO_2, (F) MnO_2/CRGO.

Fig 3. (A) Cyclic voltammograms obtained for the (a) MnO_2/GCE, (b) MnO_2/CRGO/GCE, (c) Bare GCE, (d) CRGO/GCE in 0.05 M phosphate solutions (pH 7) containing 5mM $Fe(CN)_6^{3-/4-}$ at a scan rate of 50 mV s^{-1}. (B) The Nyquist plots of the electrochemical impedance spectroscopy (EIS) for (a) Bare GCE, (b) CRGO/GCE, (c), MnO_2/CRGO/GCE, (d) MnO_2/GCE modified electrodes in PBS (pH 7) containing 5mM $Fe(CN)_6^{3-/4-}$ (1:1) in a frequency range from 0.1 Hz to 100 kHz. The inset is the Randles equivalent circuit for the modified electrodes.

Fig 4. (A) Cyclic voltammograms of 1×10^{-4} M NE and 1×10^{-4} M AC for the (a) Bare GCE, (b) MnO_2/GCE, (c) CRGO/GCE, (d) MnO_2/CRGO/GCE modified electrodes in PBS (pH 7). Scan rate: 100 mV s^{-1}. (B) SWV experiments with various concentrations of NE and AC in 0.05 M PBS (pH7). [NE]= [AC]: from a to v) 2+5, 10+10, 30+35,50+75, 100+125, 150+175, 200+225, 275+300, 300+320, 350+355, 400+400, 500+525, 600+615, 650+670, 700+750, 800+820, 850+870, 890+900, 900+925,950+960,1000+1050,1100+1125,1200+1225 µM. The insets show the linear dependence of (Ipa) peak current of NE and AC on the concentration.

Fig 5. (A) SWV experiments of the MnO_2/CRGO/GCE modified electrode in 0.05 M PBS (pH 7.0) containing 200 µM NE in the presence of 5, 10, 20,100, 175, 200, 225, 300, 350, 400, 450, 500, 525, 550, 575, 450, 500, 550, 600, 650, 680, 725, 750, 800, and 900 µM for AC. Inset:

Calibration curve for the AC concentrations *vs***.** the anodic peak currents. (B) SWV experiments for different concentrations of NE in the present of 200 µM AC by the modified electrode. NE concentrations: (a) 5, 30, 100, 200, 280, 350, 400, 450, 500, 580, 670, 710, 750, 800, 850; pH = 7 PBS. Inset: Calibration curve of the AC concentrations *vs***.** the anodic peak currents.

Fig.s

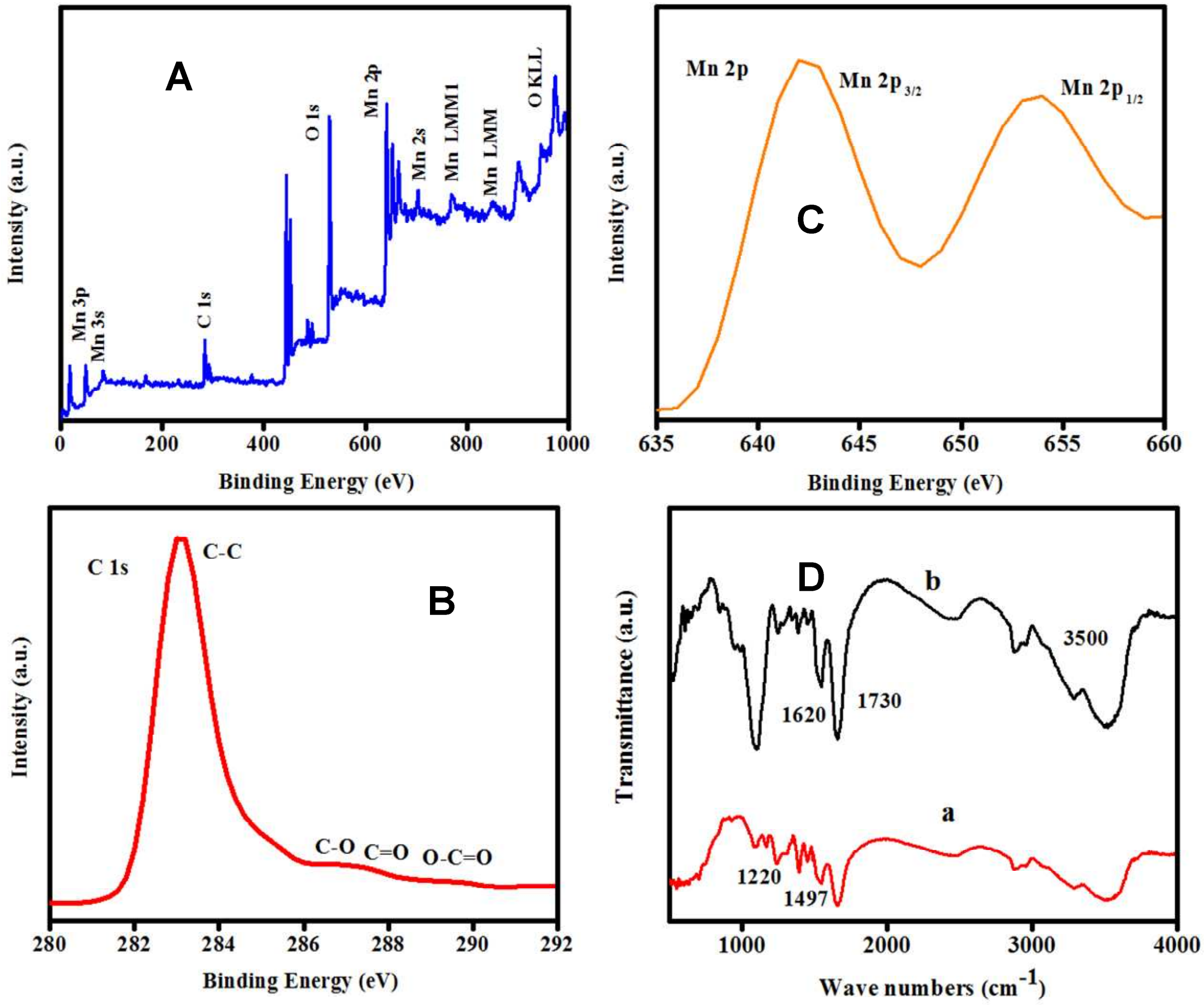
A
Intensity (a.u.)
Mn 3p
Mn 3s
C 1s
O 1s
Mn 2p
Mn 2s
Mn LMM1
Mn LMM
O KLL
0
200
400
600
800
1000
Binding Energy (eV)
C
Intensity (a.u.)
Mn 2p
Mn 2p$_{3/2}$
Mn 2p$_{1/2}$
635
640
645
650
655
660
Binding Energy (eV)
B
Intensity (a.u.)
C 1s
C-C
C-O
C=O
O-C=O
280
282
284
286
288
290
292
Binding Energy (eV)
D
Transmittance (a.u.)
b
a
1620
1730
3500
1220
1497
1000
2000
3000
4000
Wave numbers (cm^{-1})

Fig. 1

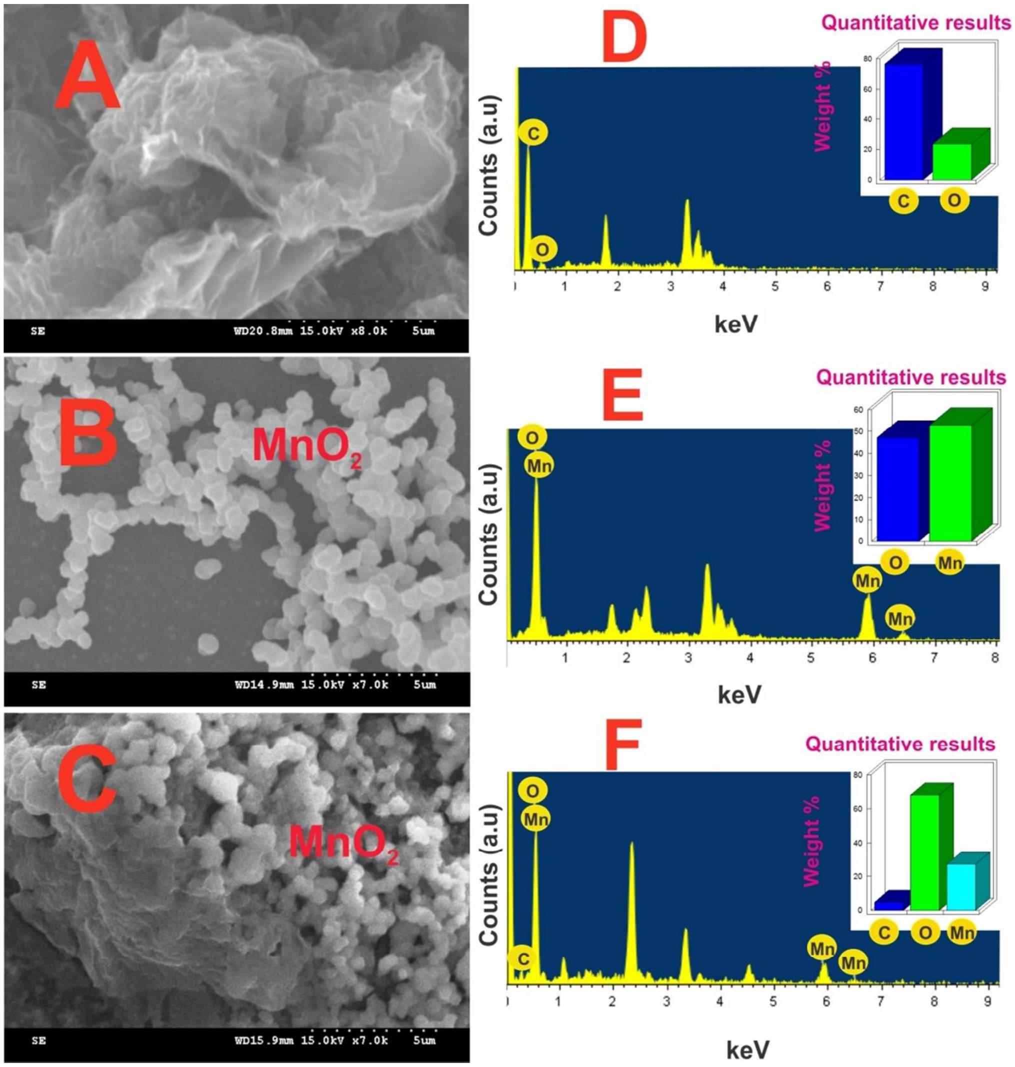
A
SE WD20.8mm 15.0kV x8.0k 5um
B
MnO$_2$
SE WD14.9mm 15.0kV x7.0k 5um
C
MnO$_2$
SE WD15.9mm 15.0kV x7.0k 5um
D
Quantitative results
Weight %
C
O
Counts (a.u)
keV
E
Quantitative results
Weight %
O
Mn
Counts (a.u)
keV
F
Quantitative results
Weight %
C
O
Mn
Counts (a.u)
keV

Fig. 2

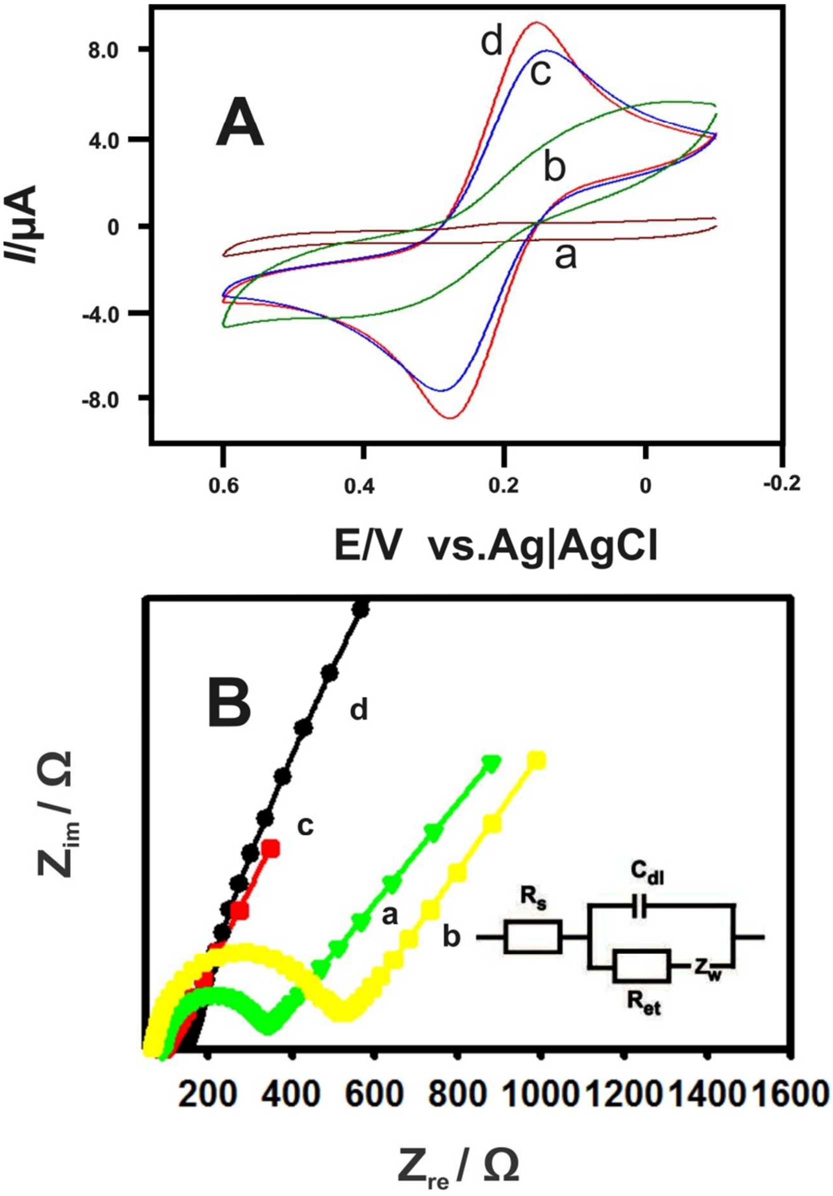
A
d
c
b
a
8.0
4.0
0
-4.0
-8.0
I/μA
0.6
0.4
0.2
0
-0.2
E/V vs.Ag|AgCl
B
d
c
a
b
Z_{im} / Ω
R_s
C_{dl}
R_{et}
Z_w
200
400
600
800
1000
1200
1400
1600
Z_{re} / Ω

Fig. 3

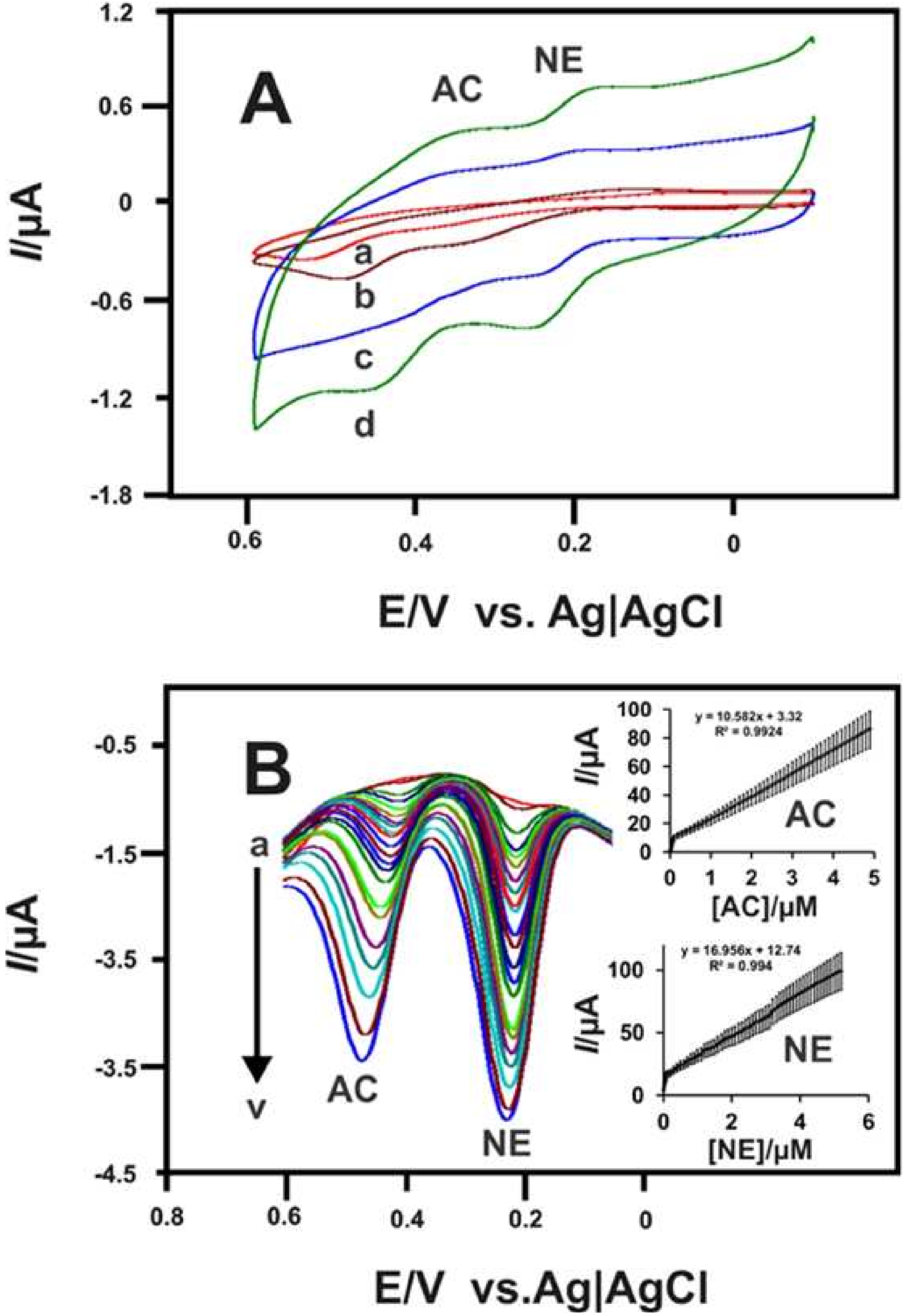
A
AC
NE
a
b
c
d
1.2
0.6
0
-0.6
-1.2
-1.8
I/µA
0.6
0.4
0.2
0
E/V vs. Ag|AgCl
B
a
v
AC
NE
-0.5
-1.5
-3.5
-3.5
-4.5
I/µA
0.8
0.6
0.4
0.2
0
E/V vs.Ag|AgCl
y = 10.582x + 3.32
R² = 0.9924
I/µA
100
80
60
40
20
0
AC
0
1
2
3
4
5
[AC]/µM
y = 16.956x + 12.74
R² = 0.994
I/µA
100
50
0
NE
0
2
4
6
[NE]/µM

Fig. 4

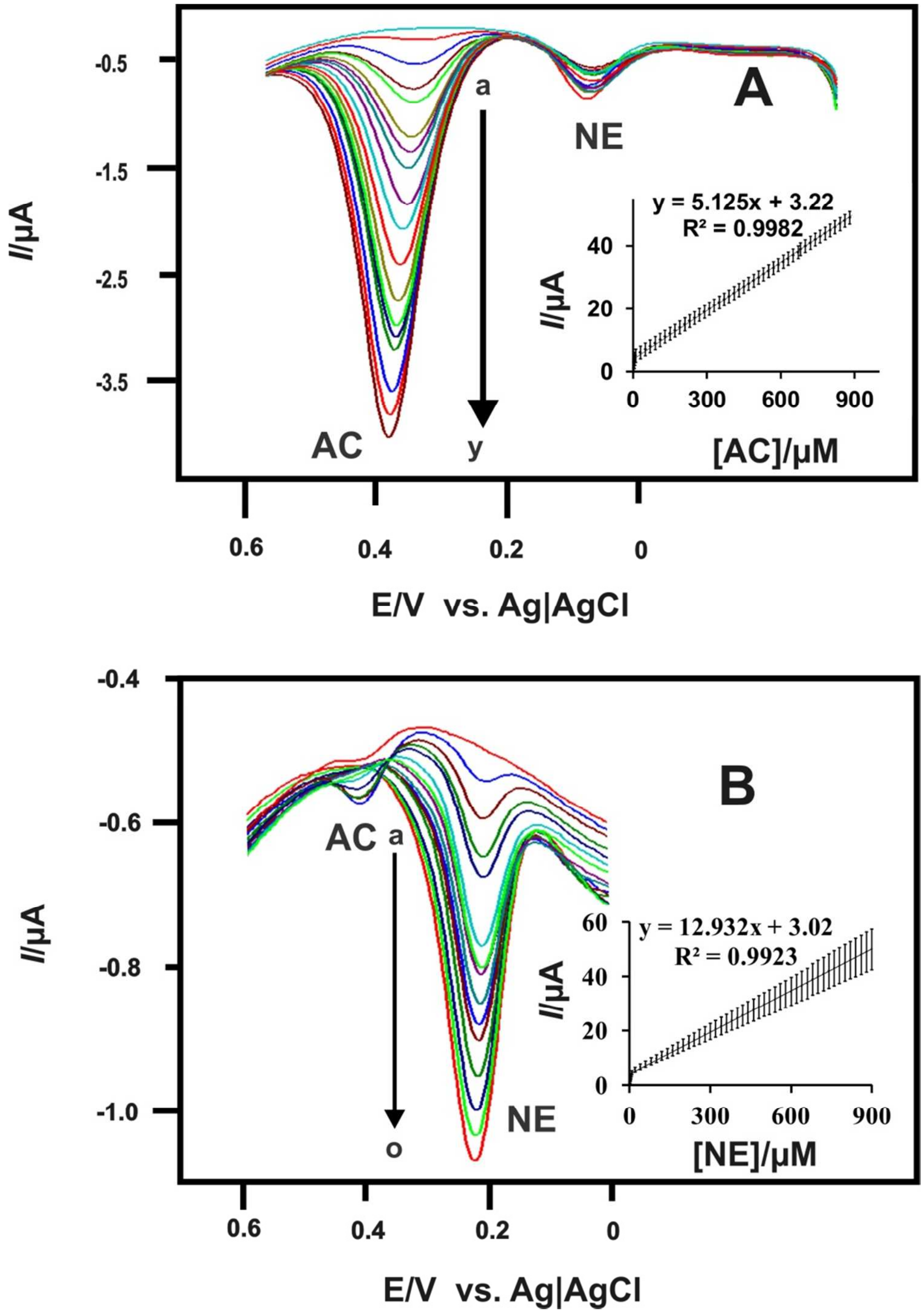
A
-0.5
-1.5
-2.5
-3.5
I/µA
a
y
NE
AC
y = 5.125x + 3.22
R² = 0.9982
40
20
0
I/µA
0
300
600
900
[AC]/µM
0.6
0.4
0.2
0
E/V vs. Ag|AgCl
B
-0.4
-0.6
-0.8
-1.0
I/µA
AC
a
o
NE
y = 12.932x + 3.02
R² = 0.9923
60
40
20
0
I/µA
0
300
600
900
[NE]/µM
0.6
0.4
0.2
0
E/V vs. Ag|AgCl

Fig. 5

Table .1.

Comparison of the efficiency of some analytical sensors used for the electro analysis of NE.

Electrode Modifier	pH	LOD (M)	Linear range (M)	Reference
2,2-[1,2 buthanediylbis(nitriloethylidyne)]-bis-hydroquinone and TiO2 nanoparticles/ Carbon paste	8.0	5.0×10^{-7}	4.0×10^{-6} to 1.1 $\times10^{-3}$	5
Calix[4]arene crown-4 ether/GCE	6.0	2.8×10^{-7}	5.5×10^{-7} to 2.3×10^{-4}	29
Carbon paste /Carbon nanotube/Ferrocene	7.0	2.1×10^{-7}	4.7×10^{-7} – 5.0×10^{-4}	30
Pd/graphene	7.2.	67 x 10^{-9}	0.0005 to 0.5 x 10^{-3}	31
benzofuran /multiwalled carbon nanotubes /ionic liquid (IL)/GCE	7.0	49 x 10^{-9}	0.1-30.0 x 10^{-6} 30.0-1000.0 x 10^{-6}	32
Hematoxylin/GCE	7.0	1.4×10^{-7}	5.0×10^{-7} to 2.742×10^{-4}	33
Carbon paste /Ferrocenemonocarboxylic acid	7.0	1.6×10^{-7}	5.2×10^{-7} to 5.3×10^{-4}	34
Graphene /GCE	7.0	4.00×10^{-7}	6.00×10^{-7} to 1.20×10^{-4}	35
Eriochrome Cyanine R	7.0	15×10^{-7}	2×10^{-6} to 50×10^{-6}	36
multi-wall carbon nanotube /CILE	7.0	9×10^{-8}	3×10^{-7} to 45×10^{-5}	37
carbon paste / 5-mino-3′,4′-dimethyl-biphenyl-2-ol (5ADB) /carbon nanotubes	7.0	5.9×10^{-7}	1.2×10^{-6} to 9.0×10^{-4}	38
Luteolin/multi-wall carbon nanotube /GCE	7.0	0.53 x 10^{-6}	0.7 x 10^{-6} to 100.0 x 10^{-6}	39
MnO_2/CRGO modified GCE	7.0	2.0×10^{-9}	2×10^{-7} to 8×10^{-4}	This work

Table. 2. Analytical application of MnO_2/CRGO modified GCE for the simultaneous determination of NE, and AC in human urine samples.

Urine sample	Added (μM)		Found (μM)		Recovery %	
	NE	AC	NE	AC	NE	AC
1	0	0	not detected	not detected	-	-
	10.0	15.0	10.2	15.2	102.0	102.3
	20.0	30.0	19.7	30.8	99.2	104.0
2	0	0	not detected	not detected	-	-
	15.0	20.0	14.4	19.8	98.2	97.6
	25.0	35.0	24.2	36.6	99.4	104.1